

Kinematics of the molecular interstellar medium probed by Gaia: steep velocity dispersion-size relation, isotropic turbulence, and location-dependent energy dissipation

Ji-Xuan Zhou,¹ Guang-Xing Li,¹  Bing-Qiu Chen,¹ 

¹ *South-Western Institute for Astronomy Research, Yunnan University, Chenggong District, Kunming 650091, P. R. China*

25 October 2021

ABSTRACT

The morphology and kinematics of the molecular interstellar medium are controlled by processes such as turbulence, gravity, stellar feedback, and Galactic shear. Using a sample of 15149 young stellar objects (YSOs) with Gaia Data Release 2 (DR2) astrometric measurements, we study morphology and kinematic structure of their associated molecular gas. We identify 150 YSO associations with distance $d \lesssim 3$ kpc. The YSO associations are oriented parallel to the disk midplane, with a median angle of 30° , and they have a median aspect ratio of 1.97. Along the Galactic longitude direction, the velocity dispersion is related to the separation by $\sigma_{v_l} = 0.58 (r_l/\text{pc})^{0.66 \pm 0.05} (\text{km s}^{-1})$, along the Galactic latitude direction, $\sigma_{v_b} = 0.54 (r_b/\text{pc})^{0.64 \pm 0.04} (\text{km s}^{-1})$, and overall $\sigma_{v,2D} = 0.74 (r/\text{pc})^{0.67 \pm 0.05} (\text{km s}^{-1})$. The slope is on the stepper side, yet consistent with previous measurements. The energy dissipation rate of turbulence $\dot{\epsilon} = \sigma_{v,3D}^3 / L$ decreases with the Galactocentric distance r_{gal} by $\dot{\epsilon} = 1.77 \times 10^{-4} e^{-0.45 (r_{\text{gal}}/\text{kpc})}$ ($\text{erg g}^{-1} \text{s}^{-1}$) for clouds with $40 \text{ pc} < r < 130 \text{ pc}$, which corresponds to a gradient of 0.2 dex kpc^{-1} . This decrease can be explained if turbulence is driven by cloud collisions, as the clouds located in the inner Galaxy have higher chances to accrete smaller clouds. Although the density structures of the complexes are anisotropic, the turbulence is consistent with being isotropic. Thus, the clouds are long-lived, stationary structures shaped by the Galactic motion where turbulence is maintained by a continuous injection.

Key words: Galaxies: ISM – ISM: structure – ISM: kinematics and dynamics – Stars: formation – Physical data and processes: turbulence

1 INTRODUCTION

The collapse of molecular clouds is a complex processes characterized by interplays between e.g. gravity, turbulence (Larson 1981) and magnetic field (Li et al. 2014). The clouds exhibit complex density and velocity structures. Larson (1981) found the velocity dispersion σ_v of a cloud is positively correlated with its size l by $\sigma_v \sim l^\beta$ where $\beta = 0.38$. The slope can be explained by the cascade of Kolmogorov-like turbulence (Kolmogorov 1941). This relation is called the Larson relation, and the role of turbulence in star formation is well-recognized ever since. However, the slope of the Larson relation remains uncertain, and the interpretation of turbulence cascade has been challenged. Solomon et al. (1987) found that the velocity dispersion σ_v of a cloud is related to its size l by $\sigma_v \sim l^{0.5}$ from 273 molecular clouds observed by the Five College Radio Astronomy Observatory (FCRAO), where the scaling exponent is larger than 0.38 as found by Larson (1981). Similar results are also reported in e.g. Bolatto et al. (2008); Heyer et al. (2009); Ballesteros-Paredes et al. (2011) proposed that the slope of the Larson relation can also be explained assuming self-gravity. Recently, Izquierdo et al. (2021)

simulated the evolution of molecular clouds in galaxy discs, and found that the exponent varies from 0.3 to 1.2.

The fact that larger velocity dispersions are found at larger scales suggests that the kinetic energy of molecular clouds is injected from the outside. To constrain turbulence injection, a promising direction is to identify coherent gas structures. Li et al. (2013) identified a kpc-sized coherent structure called the “500 pc filamentary gas wisp”, and Goodman et al. (2014) discovered an object called “extended Nessie” of a similar size. These discoveries suggest that the molecular clouds are not separated objects but an inseparable part of the Milky Way interstellar medium. Subsequent works studied samples of such filaments (Ragan et al. 2014; Abreu-Vicente et al. 2016; Wang et al. 2015; Li et al. 2016). Li et al. (2016) extracted filamentary structures from the APEX Telescope Large Area Survey of the Galaxy (ATLASGAL, Schuller et al. 2009) survey. They found that the filamentary structures tend to stay parallel to the Galactic disk mid-plane, indicating that Galactic shear plays an important role in shaping the structures of the molecular interstellar medium. Another possible consequence of shear is that it can lead to velocity anisotropy, e.g. the velocity dispersion of molecular clouds measured along the Galactic longitude l direction is larger compared to that along the Galactic latitude b direction. Koda et al. (2006) attempted to constrain the importance of shear by studying the radial velocity structures of the Boston University–Five College Radio As-

* gxli@ynu.edu.cn

† bchen@ynu.edu.cn

tronomy Observatory Galactic Ring Survey (GRS) clouds (Jackson et al. 2006), and found that the velocity gradient has no preferred direction. Whether the velocity field is isotropic or anisotropy remains unclear.

The Gaia survey (Gaia Collaboration et al. 2016) provides accurate measurements of the magnitudes, parallaxes, and proper motions of stars in the Milky Way (Gaia Collaboration et al. 2016). We use the Gaia Data Release 2 (DR2, Gaia Collaboration et al. 2018a) measurements of young stellar objects to study the kinematics of the gas they associate with. YSOs are stars at the very early stage of stellar evolution and are usually close to where they were born, such that they inhibit the velocity of gas from which they originate and their locations may indicate the shape of molecular clouds. Großschedl et al. (2021); Lim et al. (2021) compared the velocities of YSOs against the velocity of the ambient molecular gas, and found a good agreement. This technique has already been used in previous studies to study e.g. turbulent motion of molecular gas (Ha et al. 2021). Li & Chen (2021 under review) used a similar approach to study the velocity structure of a Galactic filament called the Gould Belt Radcliffe Wave (Alves et al. 2020). Using a sample of 15149 YSOs which are younger than 2 Myr and located from -6 to -10 kpc from the Galactic center, we study the kinematics of the molecular interstellar medium from several pc to one hundred pc scale.

2 DATA & METHOD

2.1 YSO data

Our YSO sample, which consists of 15149 Class I and Class II YSOs, is selected from Marton et al. (2016) obtained by applying the Support Vector Machine method to a combined dataset containing the AllWISE catalog of the Wide-field Infrared Survey Explorer (Cutri et al. 2021), the Two Micron All-Sky Survey (2MASS Cutri et al. 2003), and the Planck dust opacity values (Planck Collaboration et al. 2014). Their parallaxes and proper motions are derived by cross-matching with with Gaia DR2 (Gaia Collaboration et al. 2018b). To study the motion of gas, we choose YSOs with ages younger than 2 Myr, as the relatively young age ensures that they inherit the positions and velocities the gas they originate from (Li & Chen 2021 under review). We further remove YSOs whose parallax errors are larger than 20%.

2.2 Estimating the spatial density

We use the python function `hist3d` to produce a YSO density map in l , b , and $\log(d)$ space, where d :the distance to the Sun. Our density map has $0^\circ < l < 360^\circ$, $-25^\circ < b < 25^\circ$, $3.5 \text{ pc} < d < 7300 \text{ pc}$. We divide l into 720 bins separated by 0.5° , b into 100 bins separated by 0.5° and $\log(d)$ into 50 bins. The density map is smoothed with a Gaussian filter with $\sigma = 0.6$ pixel. The results are plotted in Fig. 1.

2.3 Identifying structures

We use the `Dendrogram` program (Rosolowsky et al. 2008) to extract structures from the YSO density map. `Dendrogram` is a program to extract structures from maps by exploiting the topological relation between isosurfaces. The results are dependent on three parameters: `min_value`, `min_delta`, and `min_npix`, where `min_value` means the minimum value to be considered as a structure, `min_delta` refers to the value difference between structures and substructures,

and `min_npix` is the smallest number of pixels contained in one structure.

Through experiments, we set `min_value = 0.1`, `min_delta = 0.3`, and `min_npix = 10`, and obtain a total of 518 structures, which contain 10 to 2593 pixels. One pixel might belong to a few nested structures. All structures found by `Dendrogram` are called “associations”. Some of the small associations are part of the larger ones, and a few examples are shown in Fig. 2. Each YSO can belong to one or a few associations, and their memberships are determined by matching their locations to the footprints of identified structures. We further remove associations that contain very few stars(≤ 15), and obtain a sample of 219 associations which are coherent in space and contain reasonable numbers of stars.

2.4 Removing Contaminations

Almost all YSO associations contain significant amounts of contaminations, as reflected from their distance distributions. To address this, by applying a Gaussian Mixture Model (`sklearn.mixture`), we decompose the distance distribution of each YSO association into a few Gaussian components, select the most prominent one, and merge it with adjacent ones if the separation is smaller than 1.5 times the dispersion. An example illustrating this procedure is plotted in Fig. 3. If more than 65% of the member YSOs are removed, the association is considered unreliable and is removed from the sample.

2.5 Final sample

We apply the following criteria to obtain a sample of YSO associations whose physical properties can be estimated reliably: (1) the number of stars is more than 20, and (2) the dispersion of distance is smaller than 0.35 kpc. Finally, we obtain a sample of 150 YSO associations, which are described in Appendix A.

The member stars have spatial distributions that resemble the molecular gas they originate from, and in the majority of the cases, their velocity distributions are Gaussian-like. One example is presented in Fig. 4, which corresponds to the well-known Orion molecular clouds. Here, we plot the distributions of member stars in the $l - b$ and $v_l - v_b$ space. In the $l - b$ space, the YSO association resembles the Orion molecular cloud, and in the velocity space, the YSOs are clustered.

2.6 Deriving physical properties

For each YSO association, we derive the following properties.

2.6.1 Distance and velocity dispersion

We use a Monte-Carlo approach to estimate the distance and velocity uncertainties. For each measurement, the uncertainties are sampled with 1000 realizations containing errors of the parallax and the proper motion. The means and dispersions of the velocities and distances can be estimated using these realizations. This allows us to derive the mean distance d_{mean} , the distance dispersion δ_d , their errors $E(d_{\text{mean}})$ and $E(\delta_d)$, the velocity dispersion along l , $\sigma_{v,l}$, the velocity dispersion of along b , $\sigma_{v,d}$, as well as the corresponding errors $E(\sigma_{v,l})$, $E(\sigma_{v,d})$.

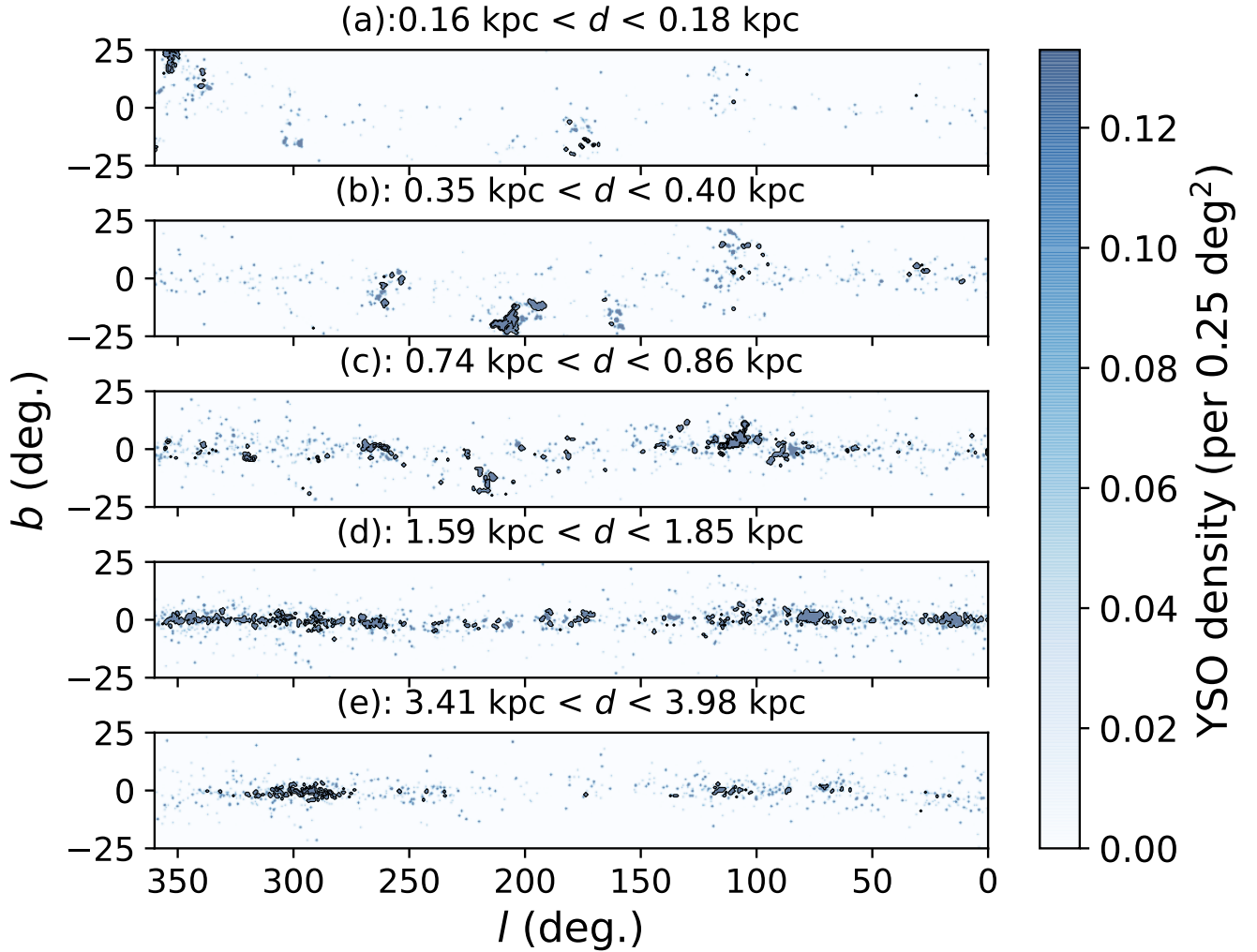


Figure 1. Spatial density of the YSO sample at five distance channels. The colors represent the YSO density, and the black contours represent the boundaries of the associations found by Dendrogram.

2.6.2 Size

The dataset allows us to study the motion along l and b directions separately. To fully exploit this potential, we derive three sizes: size in l direction - r_l , size in b direction - r_b , and overall size r . These are full width at half maxima (FWHM) widths, e.g. $r_l = 2.355d \cdot \text{std}(l_i)$, and $r_b = 2.355d \cdot \text{std}(b_i)$, where l_i, b_i are positions of the member YSOs and $\text{std}()$ calculates the standard deviation of the data. The size r is estimated using: $r = 2.355d \cdot \sqrt{(\sigma_{\min}^2 + \sigma_{\max}^2)/2}$, where $r_{\min} = \sigma_{\min} d$ and $r_{\max} = \sigma_{\max} d$, and $\sigma_{\min}, \sigma_{\max}$ are the dispersions measured along the major and minor axes of the spatial distributions on sky. d is the mean distance of every association. Our associations have sizes range from several pc to hundreds of pc. The intrinsic width of the cloud is estimated as width = $\sqrt{\text{std}(d_i)^2 - \text{std}(d_{\text{err},i})^2}$ where d_i is the distance of object i and the corresponding error is $d_{\text{err},i}$.

2.6.3 Aspect ratios and Orientations

For each association, we fit ellipses to the distribution of member YSOs in the spatial ($l - b$) and velocity ($v_l - v_b$) space by diagnosing a tensor constructed from the spatial and velocity dispersions (e.g. the tensor is $T_{i,j} = \sum p_i p_j$, where p is the spatial/velocity coordinates, and i, j represent l, b directions), and measure the orientation of the longer axes as well as aspect ratios. Spatially, we measure the position angle PA_{l-b} and the aspect ratio A_{l-b} and in the velocity space, we also measure the position angle $\text{PA}_{v_l-v_b}$ and the aspect ratio $A_{v_l-v_b}$.

3 RESULTS

3.1 Galactic distribution and size

In Fig. 5 we plot locations of the associations in the Milky Way disk, where a map of the distribution of dust from [Chen et al. \(2019a\)](#) is overlaid. The complexes are associated with dust and are organized along a few filaments. This is expected, as the YSOs are young and

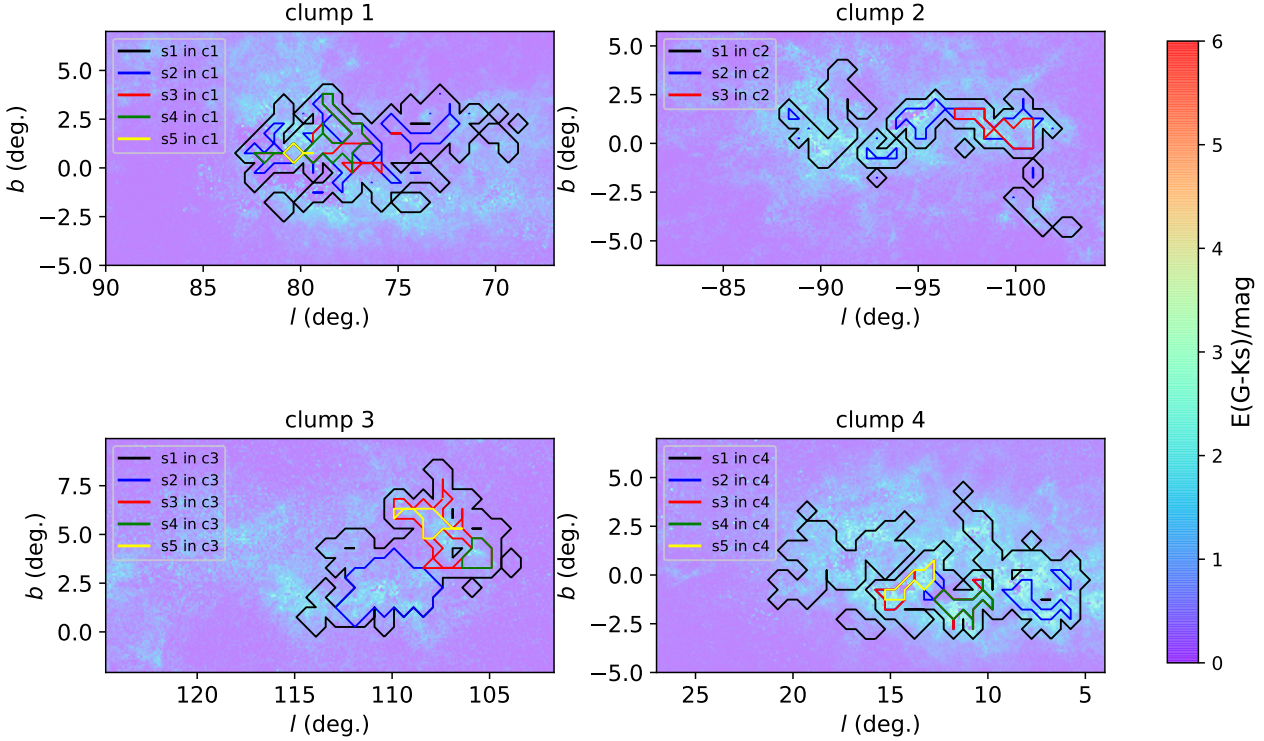


Figure 2. Examples of nested structures. The background is the 2D dust map from Chen et al. (2019a) integrated from $d = d_{\text{mean}} - \delta_d$ to $d = d_{\text{mean}} + \delta_d$, where d_{mean} is the mean distance, and δ_d is the thickness. Contours represent boundaries of the associations.

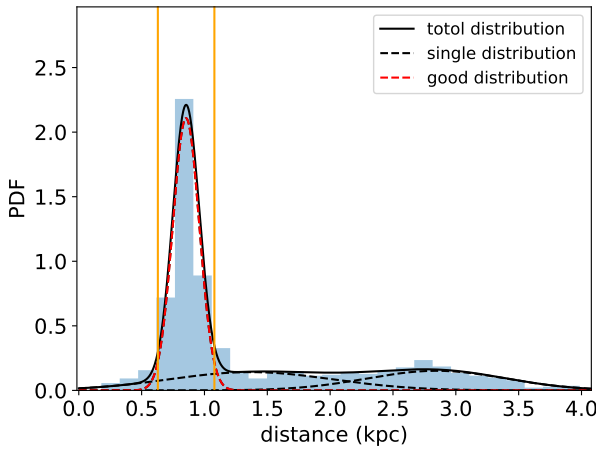


Figure 3. Generate a clean sample of member YSOs. The histogram represents the distance distribution of YSOs that belongs to one of our complexes. The solid black line refers to the overall distribution, and the dashed lines represent different Gaussian components obtained from `sklearn.mixture`. The red dashed line is the dominant component, and the two vertical orange lines mark the final distance range. Only YSOs that stay within this distance range will be considered in our analyses.

are associated with the molecular cloud which contains dust. In Fig. 5, we plot the distribution of the number of member stars contained in the complexes, as well the size distribution. The associations have sizes that range from 10 to 100 pc, which is similar to the sizes of molecular clouds obtained by e.g. Roman-Duval et al. (2010) and Chen et al. (2020).

3.2 Aspect ratio and Orientation

We plot the distributions of the position angle and aspect ratio of the ellipses respecting the distributions of member YSOs in the $l - b$ and the $v_l - v_b$ space (Fig. 6). In the $l - b$ space, the associations appear to be elongated, with a median aspect ratio of 1.97, and they tend to stay aligned with the Galactic disk mid-plane, with a median angle of 30° with respect to the mid-plane. In the $v_l - v_b$ space, the distribution has a median aspect ratio of 1.82 and a median angle of 27.7° , where the velocity dispersion is larger along the Galactic longitude. The difference between the position angle measured in space and the velocity space is also small, with a median angle difference of 24.33° .

3.3 Velocity-Size Relation, and Velocity Anisotropy

We study the relation between velocity dispersion and size using our YSO associations. This relation was proposed by Larson (1981) and is called the Larson relation. In previous studies, the velocity dispersions are estimated using the spectral lines from molecules

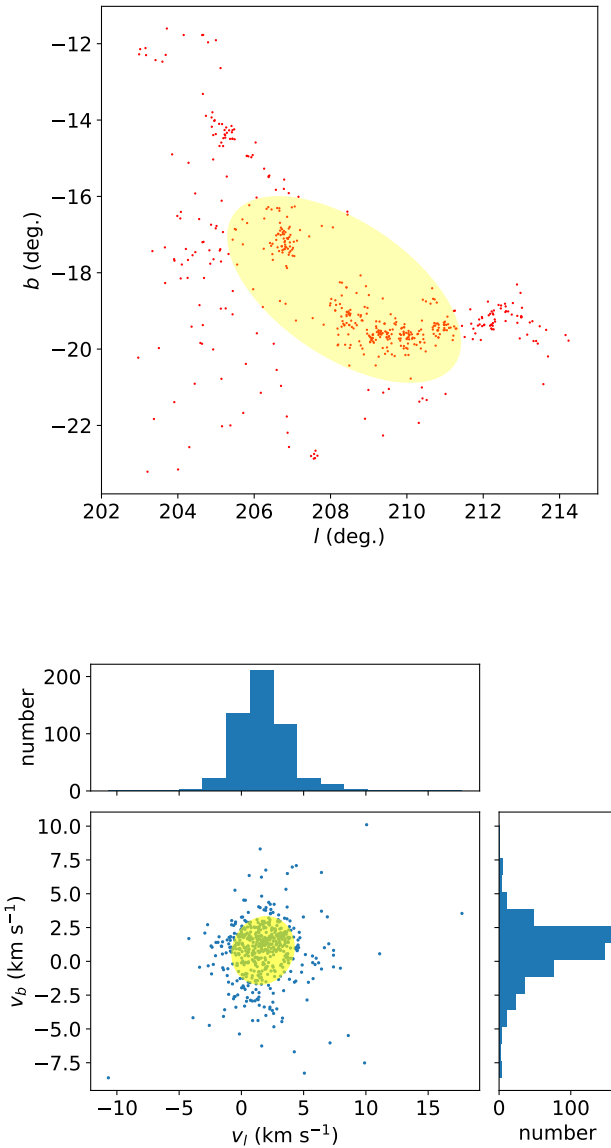


Figure 4. Locations of the member YSOs of one of our associations in the $l - b$ and $v_l - v_b$ space. Upper panel: Locations in the $l - b$ plane. Red dots are the member stars of this structure and the yellow ellipse represents the fitting result, as described in section 2.6.3, through which the aspect ratio and the orientation are measured. **Lower panel:** Locations of member YSOs in the $v_l - v_b$ space. The yellow ellipse represents the fitting result, where the heights of the ellipses are $2 r_{\min}$.

such as the CO, along the radial direction. We present a first study of the Larson relation using the Gaia proper motions. This allows us to study the relation between separation and velocity dispersion measured along l and b directions separately.

Our result is plotted in Fig. 7. Along l ,

$$\sigma_{v_l} = 0.58 (r_l/\text{pc})^{0.66} (\text{km/s}), \quad (1)$$

and along b ,

$$\sigma_{v_b} = 0.54 (r_b/\text{pc})^{0.64} (\text{km/s}). \quad (2)$$

and combining together using $\sigma_{v, 2D} = (\sigma_{v_{\min}}^2 + \sigma_{v_{\max}}^2)^{1/2}$,

$$\sigma_{v, 2D} = 0.74 (r/\text{pc})^{0.67} (\text{km/s}). \quad (3)$$

Our first finding is that the velocity dispersions measured along the l and b directions are almost identical, which means that although the density structure of the region is anisotropic, the turbulence is isotropic. To verify this, we plot the ratio between the projected length along the Galactic longitude and latitude direction r_l/r_b again the size r , and as well as the velocity dispersion ratio $\sigma_{v_l}/\sigma_{v_b}$ against the size r and find the following relation:

$$r_l/r_b \propto (r/\text{pc})^{0.22},$$

Assuming a Larson relation of $\sigma_v \propto r^{0.67}$, we have

$$\sigma_{v_l}/\sigma_{v_b} \propto (r_l/r_b)^{0.22 \times 0.67} \propto (r/\text{pc})^{0.15},$$

which is consistent with our fitting results: $\sigma_{v_l}/\sigma_{v_b} \propto r^{0.14 \pm 0.04}$. All the relations in Fig. 7 are consistent with the turbulence being isotropic.

The scaling exponent 0.67 is steeper than 0.38 in Larson (1981) but close to recent results. The slope can be explained if the turbulence is compressible (Kritsuk et al. 2013; Cen 2021), or if the turbulence is driven by accretion and gravitational contraction (e.g. Dobbs et al. 2011; Ibáñez-Mejía et al. 2016a; Izquierdo et al. 2021).

We also plotted the expected velocity dispersion assuming that the clouds contain no turbulence such that all velocities we observe come from shear by assuming a Oort constant of $A = 16.31 \pm 0.89 \text{ km s}^{-1} \text{ kpc}^{-1}$ from Wang et al. (2021) in Fig. 7. The contribution from shear to the overall velocity dispersion is negligible, even at the scale of the disk height ($H \approx 100 \text{ pc}$, e.g. Guo et al. 2021).

3.4 Energy dissipation rate in different spiral Arms

In the Kolmogorov theory of turbulence, energy injected into turbulence on large scale will dissipate on small scale. Following Mac Low (1999), we parameterize the turbulence energy dissipation rate as $\dot{\epsilon}_{\text{kin}} = \eta k \sigma_v^3$, where σ_v refers to the velocity dispersion of the cloud scale, and k is the driving wavenumber ($k \approx 1/r$). So $\dot{\epsilon} = \sigma_v^3/r$ describes the energy dissipation of molecular cloud turbulence, and here we investigate its variations with respect to their locations in the Galactic disk.

Following previous papers (Chen et al. 2019b), we separate the clouds into groups associated with different spiral arms (the Sagittarius, Local and Perseus Arm, see Fig. 4), and study the energy dissipation rate measured in terms of $\dot{\epsilon}$. Since it is hard to resolve small clouds at large distances, for each group, we select median-sized associations ($40 < r < 130 \text{ pc}$), and estimate the energy dissipation rate using $\dot{\epsilon} = \sigma_{v, 3D}^3/r$. $\sigma_{v, 3D}$ is the 3D velocity dispersion estimated using: $\sigma_{v, 3D} = \sqrt{3/2} \sigma_{v, 2D}$. Our results are plotted in the lower right panel of Fig. 5. We note that here we are deriving an un-normalized version of the energy dissipation rate, as the ‘‘true’’ energy dissipation rate is still dependent on a normalizing factor (Frisch 1995, as summarized by Qian et al. 2018), as well as the efficiency parameter η , which we can not constrain directly. We find that the energy dissipation rate decreases with increasing distance from the Galactic center. By fitting it using an exponential model we

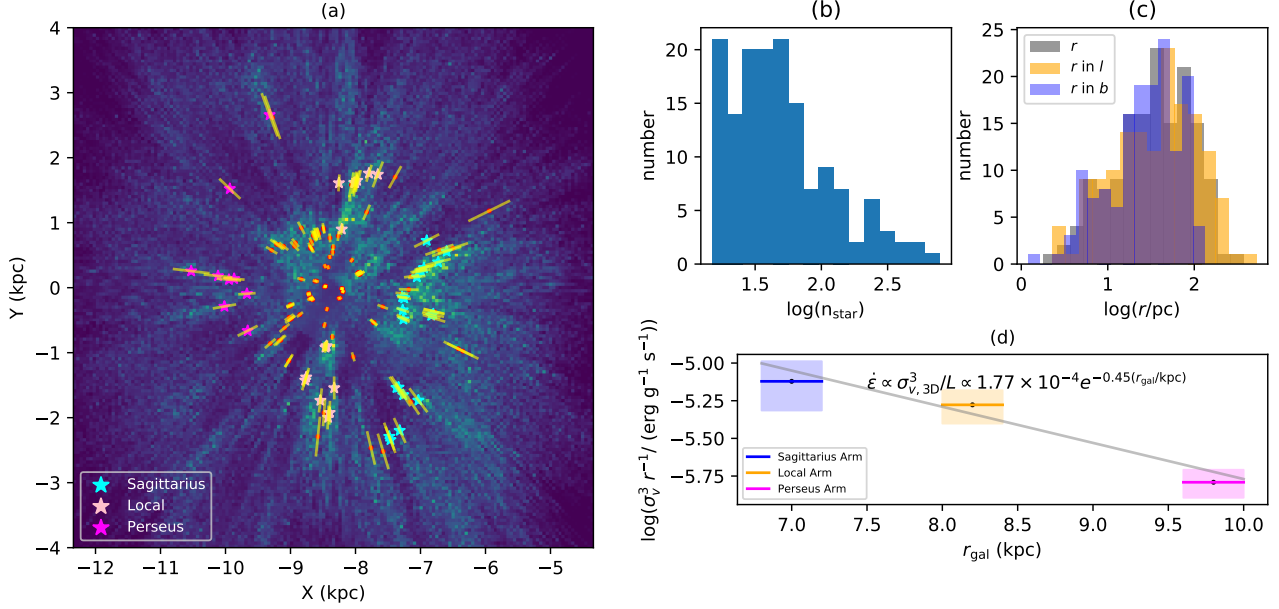


Figure 5. Properties, Galactic distribution, and energy dissipation rate of YSO associations. **Panel (a):** Location of the associations on the X-Y plane. The sun locates at (-8.34, 0) and the center of the Milky Way locates at (0, 0). Red dots represent the locations of 150 associations and yellow lines show their distance uncertainties. The background dust map is from Chen et al. (2019a). The cyan, pink, and fuchsia stars refer to the associations located on the Sagittarius Arm, the Local Arm, and the Perseus Arm respectively, and the bars represent distance uncertainties. **Panel (b):** Histogram of the number of member stars for all 150 associations. **Panel (c):** Histogram of the size of associations. The Grey one represents the distribution of the overall size, the yellow one represents the sizes measured along the Galactic longitude (I) direction, and the purple one represents the sizes measured along the Galactic latitude (b) direction. **Panel (d):** Energy dissipation rate for three spiral Arms. Fuchsia, orange and blue lines with error bars present the energy dissipation rate of associations located on the Perseus Arm, the Local Arm, and the Sagittarius Arm respectively, where the corresponding errors are also indicated using the extents of the boxes. The grey line is the fitting result where $\dot{\epsilon} = 1.77 \times 10^{-4} e^{-0.45(r_{\text{gal}}/\text{kpc})}$ ($\text{erg g}^{-1} \text{s}^{-1}$).

find $\dot{\epsilon} = 1.77 \times 10^{-4} e^{-0.45(r_{\text{gal}}/\text{kpc})}$ ($\text{erg g}^{-1} \text{s}^{-1}$) where r_{gal} is the Galactocentric distance, which implies a gradient of 0.20 dex kpc^{-1} .

4 DISCUSSIONS

4.1 Stationary, anisotropic density structures supported isotropic turbulence

The fact that we observe an isotropic turbulence despite anisotropic density structures is somewhat surprising. There are different schools of thought concerning the link between the density and velocity structures. The first believes that turbulence creates the density structure upon which collapse occurs (Vázquez-Semadeni et al. 2017). Padoan & Nordlund (2002) found the slope of the stellar (Initial Mass Function) IMF can be predicted and produced by the turbulence. The second believes that the role of turbulence is to provide support, where only gravitationally bound density fluctuations can collapse (Hennebelle & Chabrier 2008; Hopkins 2013). The third, particularly Mac Low (2003) believes that the role of supersonic turbulence is to provide support, leading to slower collapse and longer cloud lifetime. Our results favor the third one. The density structures appear to be supported by turbulence and long-lived. The conclusion is consistent with recent observational results, where the clouds can live for around 10 Myr (Kruijssen et al. 2019), longer than the crossing time of a typical cloud of 10 pc, which is around $\sim 10 \text{ pc}/3 \text{ km/s} \sim 3 \text{ Myr}$.

4.2 Energy source of molecular clouds

Our results indicate that the energy dissipation rate of turbulence decreases with the Galactocentric distance. This can be explained if the turbulence is driven by molecular cloud coagulations. Klessen & Hennebelle (2010) and Elmegreen & Burkert (2010) argued that accretion can explain the observed level of turbulence at the Galactic, molecular cloud and core scales. Using an analytical model and numerical simulations, Dobbs et al. (2011), Goldbaum et al. (2015) and Ibáñez-Mejía et al. (2016b) demonstrated that a large cloud can maintain its turbulence by accreting smaller clouds.

Li (2017) studied the co-evolution between the Galactic disk and molecular cloud, and proposed the following equation linking the properties of the disk to the energy dissipation rate of the molecular cloud:

$$\sigma_{v,\text{cloud}} \approx \sigma_{v,\text{disc}} \left(\frac{\Sigma_{\text{disc}}}{\Sigma_{\text{cloud}}} \right)^{1/3} \left(\frac{r_{\text{cloud}}}{H_{\text{disc}}} \right)^{1/3} \quad (4)$$

where $\Sigma_{\text{cloud}} \approx 10 M_{\odot} \text{ pc}^{-2}$ and is the mean surface density of the cloud, H_{disc} is the scaleheight of the disc. The level of turbulence measured in terms of $\dot{\epsilon} \propto \sigma_{v,3D}^3 / r$ is proportional to $\Sigma_{\text{disc}} / \Sigma_{\text{cloud}}$, as an increased disk surface density leads to higher chances of cloud collisions.

Miville-Deschénes et al. (2017) measured the surface density distribution of the Milky Way disk as a function of Galactocentric radius, and obtained the following equation:

$$\Sigma_{\text{disk}} \propto e^{-0.5 r_{\text{gal}}} \quad (5)$$

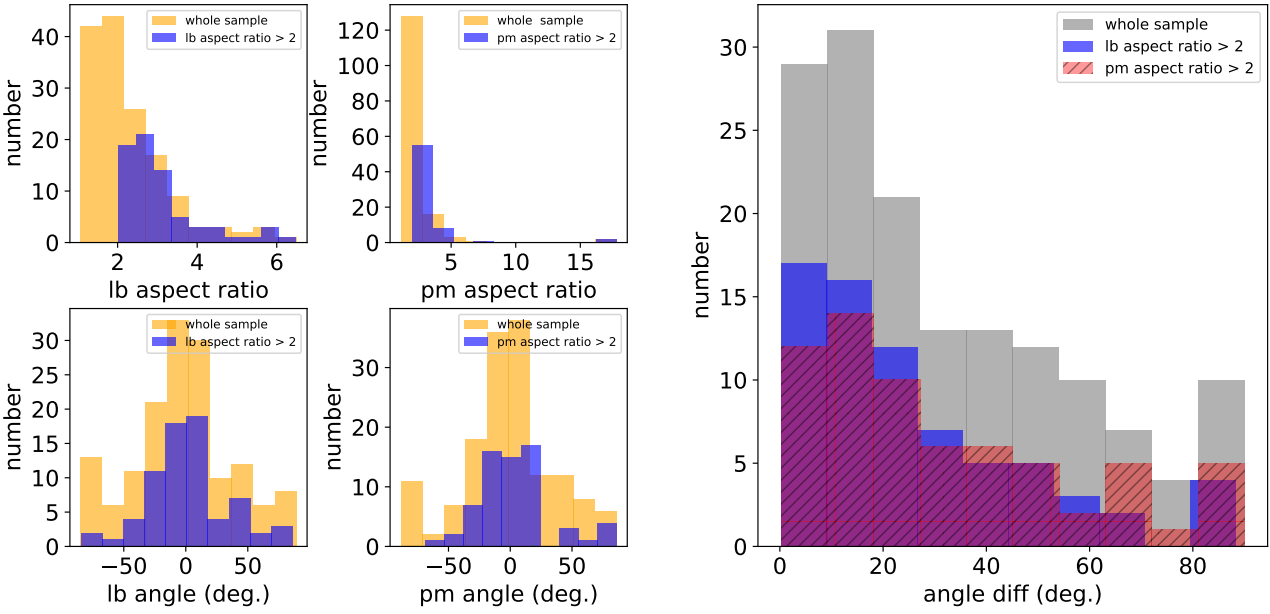


Figure 6. Left: Distributions of position angles and aspect ratios measured in the $l - b$ and $v_l - v_b$ space. The Orange histograms represent the distribution of the whole 150 structures, the purple histograms represent those with aspect ratios greater than 2, in the four figures. **Right:** Angle difference between the position angles of ellipses in the $l - b$ and $v_l - v_b$ space. Grey histogram shows the distribution of the whole sample, the blue one shows angle difference of structures with an aspect ratio greater than 2 in the $l - b$ space, and the red one with hatches represents those with an aspect ratio greater than 2 in the $v_l - v_b$ space.

Neglecting the radial variations of H_{disk} and $\sigma_{v, \text{disk}}$, according to Eq. 4, we expect

$$\dot{\epsilon} = \eta \sigma_v^3 / l \propto e^{-0.5 r_{\text{gal}}}, \quad (6)$$

which agrees with our result, where $\dot{\epsilon} \propto e^{-0.45 r_{\text{gal}}}$. The decreasing energy dissipation rate of the molecular cloud turbulence with increasing r_{gal} is likely caused by the decrease of surface density of the molecular disc, which leads to a lower collisional rate.

5 CONCLUSIONS

Using a sample of 15149 YSOs younger than 2 Myr, we extract 150 associations with sizes ranging from several pc to one hundred pc and study their velocity structures. This allows us to probe the velocities of the gas that these YSOs are associated with. Our major results include:

- (i) All the structures are elongated and are orientated parallel to the Galactic mid-plane.
- (ii) We find that the velocity and sizes are related by $\sigma_{v, 2D} = 0.74 (r/\text{pc})^{0.67 \pm 0.05} (\text{km s}^{-1})$, which is often called the Larson relation. The exponent 0.67 is consistent with recent simulation results.
- (iii) Using proper motion measurements, we study the velocity dispersion-size relation measured along the Galactic longitude and latitude separately. Along l direction, we obtain $\sigma_{v_l} = 0.58 (r_l/\text{pc})^{0.66} (\text{km s}^{-1})$ and along b direction, we obtain $\sigma_{v_b} = 0.54 (r_b/\text{pc})^{0.64} (\text{km s}^{-1})$. The results indicate that turbulence in molecular clouds is isotropic.
- (iv) Although the density structure is anisotropic, the turbulence is consistent with being isotropic. This can be explained if molecular clouds are long-lived, such that their density structures are shaped by

Galactic-scale process. During this process, turbulence is maintained by a continuous injection.

(v) We compute the energy dissipation rate of turbulence using $\sigma_{v, 3D}^3 / r$, and find it depends on the distance from the Galactic center r_{gal} , where $\dot{\epsilon} = 1.77 \times 10^{-4} e^{-0.45(r_{\text{gal}}/\text{pc})}$ (erg g $^{-1}$ s $^{-1}$), where a slope of 0.20 dex kpc $^{-1}$ is implied.

(vi) The decreasing energy dissipation rate with increasing Galactocentric radius can be explained by a reduction of clouds collisions rates, as the clouds located in the inner Galaxy where the disk surface densities are higher have higher changes of accreting smaller clouds.

ACKNOWLEDGEMENTS

This work is partially supported by the Postgraduate's Research and Innovation Project of Yunnan University (No. 2019236). GXL acknowledges supports from NSFC grant W820301904 and 12033005. BQC is supported by the National Key R&D Program of China No. 2019YFA0405500, National Natural Science Foundation of China 12173034, 11803029 and 11833006, and the science research grants from the China Manned Space Project with NO. CMS-CSST-2021-A09, CMS-CSST-2021-A08 and CMS-CSST-2021-B03.

This work presents results from the European Space Agency (ESA) space mission Gaia. Gaia data are being processed by the Gaia Data Processing and Analysis Consortium (DPAC). Funding for the DPAC is provided by national institutions, in particular the institutions participating in the Gaia MultiLateral Agreement (MLA). The Gaia mission website is <https://www.cosmos.esa.int/gaia>. The Gaia archive website is <https://archives.esac.esa.int/gaia>. This research has used ASTRODENDRO, a PYTHON package to compute dendrograms of Astronomical data (<http://www.dendrograms.org/>).

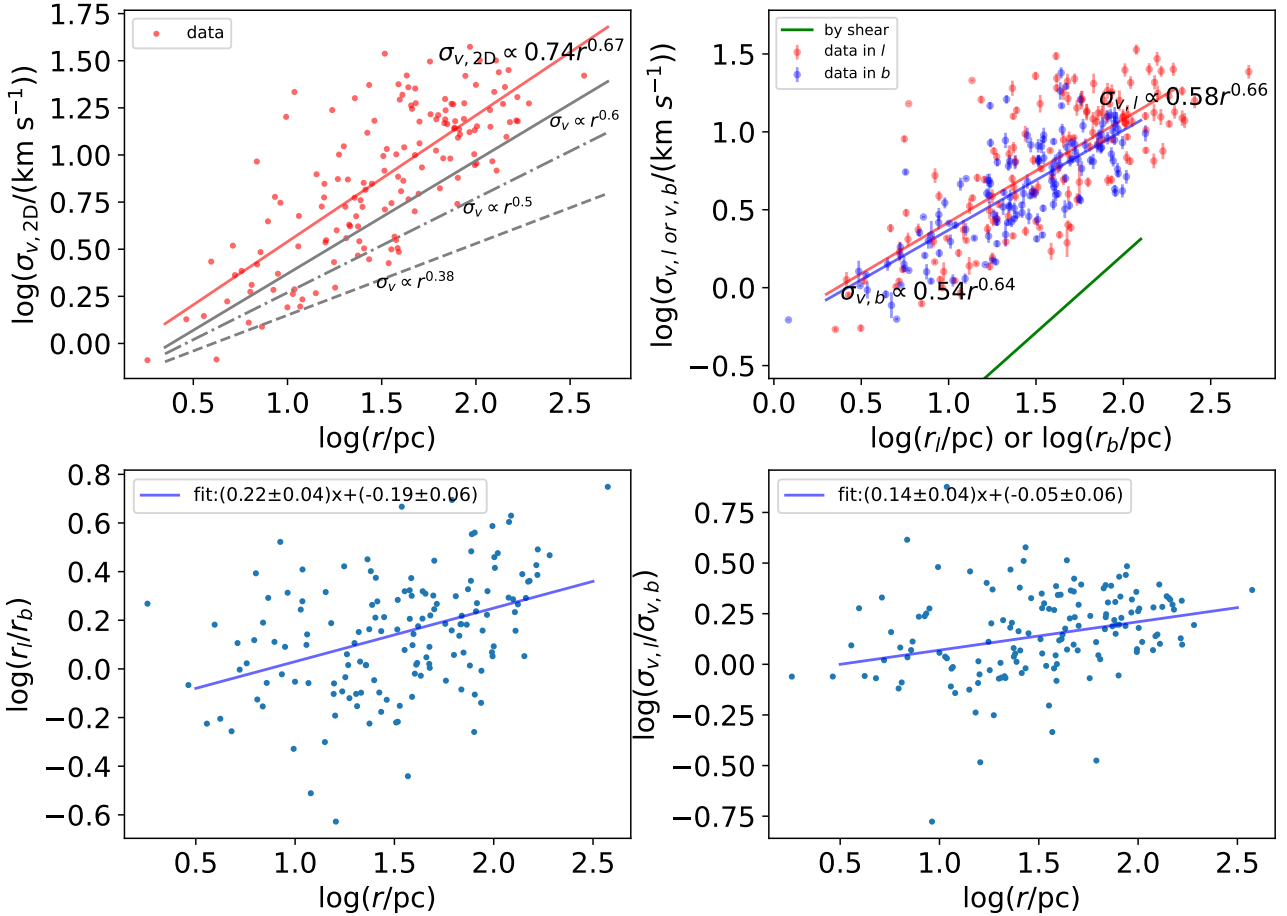


Figure 7. Relation between velocity and size. **Upper left:** $\log(\sigma_{v,2D})$ vs $\log(r)$. Red dots are the combined 2D structure data and the red line is the fitting result to the data points: $y = (0.67 \pm 0.05)x + (-0.13 \pm 0.08)$. **Upper right:** $\log(\sigma_{v,l})$ vs $\log(r_l)$ and $\log(\sigma_{v,b})$ vs $\log(r_b)$. Red dots are the data in *l* direction and red line is the fitting result: $y = (0.66 \pm 0.05)x + (-0.24 \pm 0.08)$. Blue dots are the data in *b* direction and the blue line is the fitting result: $y = (0.64 \pm 0.04)x + (-0.27 \pm 0.06)$. The green line shows the velocity dispersion that can be provided by Galactic shear. **Lower left:** $\log(r_l/r_b)$ vs $\log(r)$. Blue dots are our data and the blue line is the fitting result: $y = (0.22 \pm 0.04)x + (-0.19 \pm 0.06)$. **Lower right:** $\log(\sigma_{v,l}/\sigma_{v,b})$ vs $\log(r)$. Blue dots are our data and the blue line is the fitting result: $y = (0.14 \pm 0.04)x + (-0.05 \pm 0.06)$.

DATA AVAILABILITY

The paper makes use of published data from Marton et al. (2016) and Gaia DR2 (Gaia Collaboration et al. 2018b). Our Table A1 will be made available online upon publication.

REFERENCES

Abreu-Vicente J., Ragan S., Kainulainen J., Henning T., Beuther H., Johnston K., 2016, [A&A](#), **590**, A131

Alves J., et al., 2020, [Nature](#), **578**, 237

Ballesteros-Paredes J., Hartmann L. W., Vázquez-Semadeni E., Heitsch F., Zamora-Avilés M. A., 2011, [MNRAS](#), **411**, 65

Bolatto A. D., Leroy A. K., Rosolowsky E., Walter F., Blitz L., 2008, [ApJ](#), **686**, 948

Cen R., 2021, [ApJ](#), **906**, L4

Chen B. Q., et al., 2019a, [MNRAS](#), **483**, 4277

Chen B. Q., et al., 2019b, [MNRAS](#), **487**, 1400

Chen B. Q., et al., 2020, [MNRAS](#), **493**, 351

Cutri R. M., et al., 2003, 2MASS All Sky Catalog of point sources.

Cutri R. M., et al., 2021, VizieR Online Data Catalog, p. II/328

Dobbs C. L., Burkert A., Pringle J. E., 2011, [MNRAS](#), **413**, 2935

Elmegreen B. G., Burkert A., 2010, [ApJ](#), **712**, 294

Frisch U., 1995, Turbulence. The legacy of A.N. Kolmogorov

Gaia Collaboration et al., 2016, [A&A](#), **595**, A1

Gaia Collaboration et al., 2018a, [A&A](#), **616**, A1

Gaia Collaboration et al., 2018b, [A&A](#), **616**, A1

Goldbaum N. J., Krumholz M. R., Forbes J. C., 2015, [ApJ](#), **814**, 131

Goodman A. A., et al., 2014, [ApJ](#), **797**, 53

Großschedl J. E., Alves J., Meingast S., Herbst-Kiss G., 2021, [A&A](#), **647**, A91

Guo H. L., et al., 2021, [ApJ](#), **906**, 47

Ha T., Li Y., Xu S., Kounkel M., Li H., 2021, [ApJ](#), **907**, L40

Hennebelle P., Chabrier G., 2008, [ApJ](#), **684**, 395

Heyer M., Krawczyk C., Duval J., Jackson J. M., 2009, [ApJ](#), **699**, 1092

Hopkins P. F., 2013, [MNRAS](#), **430**, 1653

Ibáñez-Mejía J. C., Mac Low M.-M., Klessen R. S., Baczynski C., 2016a, [ApJ](#), **824**, 41

Ibáñez-Mejía J. C., Mac Low M.-M., Klessen R. S., Baczynski C., 2016b, [ApJ](#), **824**, 41

Izquierdo A. F., et al., 2021, [MNRAS](#), **500**, 5268

Jackson J. M., et al., 2006, [ApJS](#), **163**, 145
 Klessen R. S., Hennebelle P., 2010, [A&A](#), **520**, A17
 Koda J., Sawada T., Hasegawa T., Scoville N. Z., 2006, [ApJ](#), **638**, 191
 Kolmogorov A. N., 1941, Doklady Akademii Nauk Sssr, 31
 Kristsuk A. G., Lee C. T., Norman M. L., 2013, [MNRAS](#), **436**, 3247
 Kruijssen J. M. D., et al., 2019, [Nature](#), **569**, 519
 Larson R. B., 1981, [MNRAS](#), **194**, 809
 Li G.-X., 2017, [MNRAS](#), **471**, 2002
 Li G.-X., Wyrowski F., Menten K., Belloche A., 2013, [A&A](#), **559**, A34
 Li H. B., Goodman A., Sridharan T. K., Houde M., Li Z. Y., Novak G., Tang K. S., 2014, in Beuther H., Klessen R. S., Dullemond C. P., Henning T., eds, Protostars and Planets VI. p. 101 ([arXiv:1404.2024](#)), doi:10.2458/azu_uapress_9780816531240-ch005
 Li G.-X., Urquhart J. S., Leurini S., Csengeri T., Wyrowski F., Menten K. M., Schuller F., 2016, [A&A](#), **591**, A5
 Lim W., et al., 2021, [PASJ](#), **73**, S239
 Mac Low M.-M., 1999, [ApJ](#), **524**, 169
 Mac Low M. M., 2003, MHD Turbulence in Star-Forming Regions and the Interstellar Medium. pp 182–212
 Marton G., Tóth L. V., Paladini R., Kun M., Zahorecz S., McGehee P., Kiss C., 2016, [MNRAS](#), **458**, 3479
 Miville-Deschénes M.-A., Murray N., Lee E. J., 2017, [ApJ](#), **834**, 57
 Padoa P., Nordlund Å., 2002, [ApJ](#), **576**, 870
 Planck Collaboration et al., 2014, [A&A](#), **571**, A16
 Qian L., Li D., Gao Y., Xu H., Pan Z., 2018, [ApJ](#), **864**, 116
 Ragan S. E., Henning T., Tackenberg J., Beuther H., Johnston K. G., Kainulainen J., Linz H., 2014, [A&A](#), **568**, A73
 Roman-Duval J., Jackson J. M., Heyer M., Rathborne J., Simon R., 2010, [ApJ](#), **723**, 492
 Rosolowsky E. W., Pineda J. E., Kauffmann J., Goodman A. A., 2008, The Astrophysical Journal, 679
 Schuller F., et al., 2009, [A&A](#), **504**, 415
 Solomon P. M., Rivolo A. R., Barrett J., Yahil A., 1987, [ApJ](#), **319**, 730
 Vázquez-Semadeni E., González-Samaniego A., Colín P., 2017, [MNRAS](#), **467**, 1313
 Wang K., Testi L., Ginsburg A., Walmsley C. M., Molinari S., Schisano E., 2015, [MNRAS](#), **450**, 4043
 Wang F., Zhang H. W., Huang Y., Chen B. Q., Wang H. F., Wang C., 2021, [MNRAS](#), **504**, 199

APPENDIX A: PARAMETERS OF ASSOCIATIONS

In Table A1, we list the properties of the associations, including the mean longitude, the mean latitude, the number of the member stars, the mean distance, the position angle, and aspect ratio in $l - b$ and $v_l - v_b$ space, the angle difference between $l - b$ and $v_l - v_b$ space, the velocity dispersion in l and b directions, the combined 2D velocity dispersion, the size in l and b directions, and the combined size of some of the 150 associations.

Table A1: Parameters of YSO associations (only a fraction of the table is shown and the full table can be downloaded online).

id	$l(^{\circ})$	$b(^{\circ})$	n_{star}	$d(\text{kpc})$	$\text{PA}_{\nu_L - \nu_B}(^{\circ})$	$\text{A}_{\nu_L - \nu_B}$	$\text{PA}_{l-b}(^{\circ})$	A_{l-b}	$\Delta_{\text{A}}(^{\circ})$	$\sigma_{\nu_L}(\text{km/s})$	$\sigma_{\nu_B}(\text{km/s})$	$\sigma_{\nu,2D}(\text{km/s})$	$r_l(\text{pc})$	$r_b(\text{pc})$	$r(\text{pc})$
0	171.67	-15.46	62	0.13	-41.33	1.70	10.25	2.89	51.57	1.33	1.94	14.36	5.60	10.90	
1	169.56	-15.70	33	0.13	-33.19	1.62	11.71	2.87	44.90	1.46	1.88	8.32	3.37	6.35	
2	168.68	-15.88	24	0.13	-64.20	1.30	-84.77	1.17	20.57	0.90	1.03	2.67	3.12	2.90	
3	174.47	-15.00	45	0.14	57.49	1.79	-63.54	1.66	58.96	1.31	1.61	2.05	5.47	7.30	6.45
4	338.20	8.99	47	0.16	-25.54	2.96	14.48	6.49	40.03	1.67	0.96	1.92	11.40	3.43	8.42
5	336.42	8.56	21	0.16	-25.40	4.07	28.86	2.59	54.26	2.41	1.27	2.72	4.65	3.06	3.94
6	339.67	9.35	24	0.16	-71.61	1.22	3.45	1.87	75.06	0.54	0.62	0.82	2.25	1.21	1.81
7	352.88	19.48	255	0.14	-76.84	1.43	-84.38	2.04	7.54	1.12	1.50	1.85	8.94	17.87	14.13
8	353.26	18.91	166	0.14	-76.76	1.49	86.00	3.33	17.24	1.01	1.41	1.71	5.00	16.21	11.99
9	353.20	17.01	107	0.14	-76.26	1.23	82.05	1.86	21.68	1.10	1.29	1.67	3.28	5.92	4.79
10	353.38	22.47	68	0.14	-84.42	1.36	24.80	1.55	70.78	0.79	1.04	1.29	7.00	5.33	6.23
11	297.06	-15.25	59	0.19	-15.30	1.27	-71.88	1.97	56.58	1.12	0.91	1.40	2.60	4.37	3.60
12	303.58	-14.67	24	0.20	54.32	1.71	70.31	1.91	15.98	0.55	0.63	0.82	3.14	5.04	4.20
13	158.45	-20.74	49	0.30	-12.48	1.47	41.79	1.67	54.27	2.05	1.42	2.43	5.86	5.55	5.71
14	160.34	-17.94	33	0.32	12.45	2.42	24.01	1.46	11.56	3.02	1.41	3.30	5.71	4.47	5.13
15	104.42	14.02	18	0.33	10.70	1.36	-21.06	2.92	31.76	1.00	0.77	1.23	9.22	4.71	7.32
16	208.36	-18.44	525	0.39	43.87	1.11	-34.06	1.98	77.94	2.18	2.18	3.06	43.11	34.42	39.01
17	210.08	-19.48	285	0.39	-8.20	1.31	0.16	2.64	8.36	2.15	1.66	2.70	23.35	8.84	17.66
18	205.96	-16.34	155	0.40	60.32	1.36	-68.98	1.64	50.70	2.38	2.77	3.62	16.68	23.74	20.52
19	206.43	-16.96	79	0.40	61.76	1.62	13.14	1.29	48.62	2.01	2.59	3.27	12.62	10.05	11.41
20	205.28	-14.37	39	0.42	40.47	1.60	-45.26	2.88	85.72	1.70	1.63	2.31	5.24	5.28	5.26
...
130	346.74	1.00	101	1.60	-28.41	1.79	-4.07	2.72	24.34	12.25	9.11	15.24	217.07	81.27	163.90
131	345.22	0.78	89	1.59	-36.42	1.82	-19.67	2.71	16.75	13.29	11.31	17.33	149.76	76.25	118.83
132	344.16	1.22	60	1.57	-41.15	2.44	-31.19	1.34	9.96	12.12	10.94	16.27	67.09	58.77	63.07
133	352.35	2.80	42	1.07	-14.24	3.12	15.38	1.66	29.61	18.38	7.47	19.82	81.20	53.16	68.63
134	335.75	-1.52	29	1.18	-18.60	1.57	-13.47	4.44	5.12	11.40	8.05	13.97	103.57	34.02	77.09
135	333.95	0.30	45	2.14	9.22	2.69	-11.50	1.81	20.72	29.47	11.89	31.73	156.06	91.16	127.80
136	336.75	-1.76	24	1.17	51.30	1.58	8.57	1.97	42.73	4.41	4.87	6.54	32.45	17.13	25.95
137	333.89	0.20	33	2.22	6.82	1.96	-10.00	1.94	16.83	24.49	12.75	27.47	164.54	89.27	132.37
138	304.11	0.55	80	2.12	-2.50	1.96	-12.91	2.67	10.40	25.21	12.79	28.21	193.07	84.52	149.03
139	307.05	-0.01	15	2.17	-74.32	1.21	-14.62	1.65	59.70	20.44	23.93	31.31	67.57	44.08	57.04
140	303.06	0.80	45	1.97	1.84	3.09	3.25	1.44	1.42	24.95	8.18	26.29	102.03	70.97	87.88
141	303.19	1.13	29	1.83	16.21	1.69	1.25	3.59	14.96	12.92	8.24	15.11	105.70	29.52	77.60
142	302.24	1.14	18	1.82	15.23	1.84	12.35	2.27	2.88	16.00	9.50	18.32	57.55	28.22	45.32
143	294.92	-1.39	34	2.42	13.43	1.81	-78.52	1.24	88.05	13.61	7.96	15.45	61.76	75.06	68.73
144	290.58	0.42	62	2.44	-4.39	1.53	-77.95	1.43	73.55	13.20	8.53	15.54	71.74	98.90	86.39
145	290.56	-0.12	39	2.50	-3.26	1.47	-17.88	1.71	14.62	12.43	8.33	14.75	80.48	52.72	68.03
146	283.20	-1.88	38	2.53	14.37	3.78	51.64	1.08	37.27	18.01	6.52	18.82	85.97	87.49	86.74
147	286.91	-0.67	27	2.63	-20.02	1.78	-13.04	2.43	6.98	15.91	10.33	18.69	95.00	44.67	74.23
148	86.98	3.93	16	1.62	18.88	1.70	47.99	2.06	29.11	22.07	14.70	26.40	41.54	44.31	42.94